An Experimental Investigation of Distributed Acoustic Sensing (DAS) on Lake Ice

Ethan Castongia[1]*, Herb F. Wang[2], Neal Lord[2], Dante Fratta[3], Michael Mondanos[4] and Athena Chalari[5]
[1]Geoscience, University of Wisconsin-Madison*, 700 G. St. ATO 1286, Anchorage, AK 99501 U.S.A.
Email: castongia5@hotmail.com
[2]Geoscience, University of Wisconsin-Madison, Madison, WI 53706 U.S.A.
[3]Geological Engineering, University of Wisconsin-Madison, Madison, WI 53706 U.S.A.
[4]VP-Industrial Applications. Silixa Ltd., Elstree, Hertfordshire, U.K.
[5]Environmental Engineer. Silixa Ltd., Elstree, Hertfordshire, U.K.

ABSTRACT

A vibration-sensitive, Distributed Acoustic Sensor (DAS) array, using fiber-optic cables, was deployed in a triangularly shaped geometry on the frozen surface of Lake Mendota in Madison, Wisconsin, USA. The purpose of the array and testing program was to analyze the DAS response and to utilize the high spatial density of the distributed array for system response characterization in a well-constrained, small, surface array. A geophone array was also deployed to provide a reference system. The design of the array allowed us to assess the response of DAS with respect to distance from the seismic sources, the degradation of the response with length of the cable, the directivity of the fiber response with respect of the direction of the particle motion, and the quality of the signal with respect to cable type. The DAS array was examined for different cable constructions and orientations relative to the source propagation direction. Tight-buffered and loose-tube fiber-optic cable constructions were used, with both having good signal responses when well-coupled to the ice. In general, the tight-buffered cable was better suited for DAS applications. Directional sensitivity of the DAS was also inspected for several directions of wave propagation and particle motion. The results showed that the strongest DAS signals were recorded when the direction of the fiber was oriented parallel to the direction of particle motion. Finally, the DAS and geophone data sets were examined together to qualitatively determine, in conjunction with established DAS best practices, how the high spatial density offered by DAS could improve results over traditional point sensor arrays in certain situations.

Introduction

Distributed Acoustic Sensing (DAS) records passing elastic waves along the length of a fiber-optic cable by using an interrogator unit to generate a series of laser pulses and sensing the backscattering of the light along the length of the fiber. The unit interprets the backscattered light signatures for strain rate. DAS is an emerging fiber-optic sensing technology similar to Distributed Temperature Sensing (DTS) and Distributed Temperature and Strain Sensing (DTSS) in that the fiber-optic cable itself is the sensor (Mestayer *et al*., 2011; Miller *et al*., 2012). Continuous sensing over one kilometer with a spatial sampling distance of one meter makes DAS the equivalent of a thousand seismic sensors spaced every meter. A single DAS interrogator can provide sensing for cable distances up to 100-km in length with negligible signal-to-noise degradation using optical amplifiers (Parker *et al*., 2014). This capability can be exploited for near-surface geophysical surveys on land and ice, wherever fiber-optic cables can be embedded and coupled to the subsurface. The dense spatial sensing and high sampling rate capabilities of DAS have the potential for major advances relative to existing methods in applications such as explosion and rock burst detection, local earthquake detection, seismic monitoring, and tomographic imaging of the near subsurface.

DAS has been implemented in boreholes for long-term, repeat vertical seismic profiles (Madsen *et al*. 2012; Daley *et al*. 2013; Mateeva *et al*. 2014b; Daley *et al*., 2015), for flow monitoring (Johannessen *et al*., 2012; Parker *et al*., 2014) and for hydraulic fracture imaging (Molenaar *et al*. 2012). DAS deployments in surface

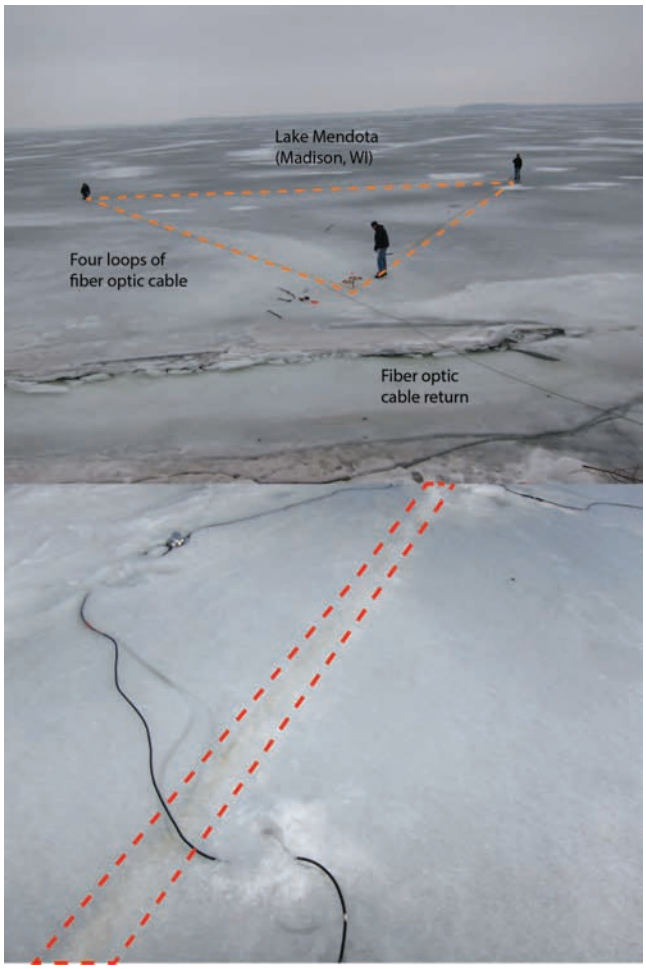

Figure 1. Top: Photo of the fiber-optic cable array being deployed on the ice in frozen Lake Mendota. Each person is standing roughly at a vertex of the equilateral triangular array. The dashed line in the background highlights the array. Bottom: Photo of one of the array sides showing uniform cable-to-ice coupling located within dashed trapezoid.

arrays on land have been reported by Daley *et al*. (2013) and Mellors *et al*. (2014) and by the University of Wisconsin-Madison group (Baldwin *et al*., 2014; Lancelle *et al*. 2014; Wang *et al*. 2014; Lord *et al*. 2016). Potential applications exist for DAS surveys on the Greenland or Antarctic ice sheets where seismic surveys are run periodically over many years to observe long-term changes in ice structure (Eisen *et al*., 2010). With these applications in mind, a field trial of DAS was conducted in March 2012 using a triangularly shaped array on the frozen surface of Lake Mendota next to the Limnology building on the University of Wisconsin-Madison campus (Fig. 1). The principal purpose of the testing program was to assess the ability of DAS to measure elastic wave fields. In addition, we wished to characterize the DAS waveforms in the context of known measurements of the elastic field. We accomplished these objectives by deploying a standard geophone array at 5-meter spacing adjacent to the fiber-optic cable as a reference.

Distributed Acoustic Sensing

DAS senses strain rates by capturing changes in Rayleigh scattering caused by deformations in the fiber between consecutive laser pulses. The backscattered energy is related to the density of particles, which is changed by strain variations along the fiber optic core. Thus, the fiber itself becomes a distributed array with nearly continuous sensing abilities in both space and time (Miller *et al*., 2012; Daley *et al*., 2013; Parker *et al*., 2014). The instrument specifications state that it can interrogate each meter of 100 km of fiber at a sampling rate of up to 10 kHz. The proprietary Intelligent Distributed Acoustic Sensor (iDAS) system, manufactured by Silixa Ltd., digitally records both the amplitude and phase of the elastic-wave field at ten-meter gauge length with a dynamic range of more than 120 dB and no cross-talk. The gage length is the base line distance for DAS obtaining length changes. It represents the spatial resolution. The 0.5 m or 1.0 m distance between channels is the spatial sampling distance, as distinct from the spatial resolution. (Johannessen *et al*., 2012; Miller *et al*., 2012). Because the iDAS interrogator records both amplitude and phase over a broad dynamic range, the interrogator can produce time-series data that are linearly related to the strain along the fiber core (Miller *et al*., 2012). Instrument sensitivity can be improved by array design that, *e.g*., loops the cable such that the same physical location has multiple strands of the cable passing over it (Parker *et al*., 2012; Daley *et al*. 2015).

DAS Field Trial on Lake Mendota

We constructed an array in the shape of an equilateral triangle with a side length of 30 meters on frozen Lake Mendota (Fig. 1). The ice thickness varied from 0.15 to 0.20 m at the time of the test. Several centimeters of fresh snow fell on the cable shortly after it was laid on the ice. By the time testing began three days later, the cables were frozen into the ice at a depth of about 1 to 2 cm, as a result of which, we had mostly uniform cable-ice coupling. The ice conditions were important to note as the expected range of velocities for thick solid ice is between 3,432 and 3,698 m/s (Ewing

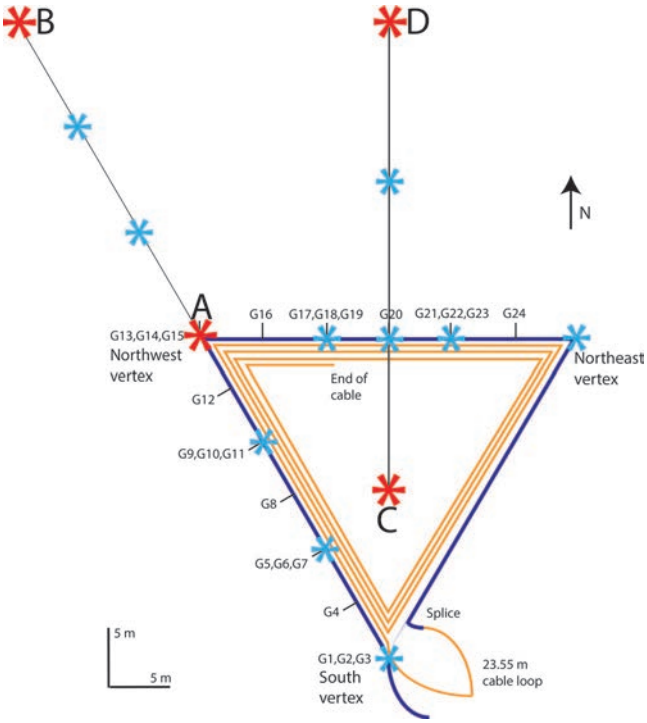

Figure 2. Sketch of the entire array layout. Each side is 30 m long. The thicker lines represent tight-buffered cable, and the thinner lines represent multiple wraps of loose-tube cable. The symbol "*" corresponds to a source location, where a darker (or red) "*" symbol with a letter label is a source location for which data are presented in this paper. Locations with multiple geophones represent three components whereas location with a single geophone is a vertical sensor.

and Crary, 1934), whereas a range between 2,000 and 3,040 m/s is expected for thinner ice layers (Wen *et al*., 1991).

Manufacturers offer dozens of fiber-optic cable constructions for different applications. Almost any kind of fiber-optic cable will respond to elastic waves, but some are better than others for recording strain. Our trial compared the response between two major fiber-optic cable types. The first type was a tight-buffered single mode fiber-optic cable, which accounted for the first 111 m of cable in the array. The second type was a loose-tube single mode fiber-optic cable, which was spliced to the first cable and added 332 m of length to the continuous cable array (Fig. 2). Tight-buffered fiber is typically used for Distributed Temperature and Strain Sensing (DTSS) and loose-tube fiber for Distributed Temperature Sensing (DTS).

In total, the continuous DAS cable was looped approximately four times around the triangular array to obtain multiple readings at each sampling location. The complete array consisted of about 443 m of continuous cable length. The fiber-optic cable was terminated and capped 10.45 m east of the Northwest vertex. The design of the array allowed us to assess the response of DAS with respect to distance from different seismic source locations, the degradation of the response with length of the cable, the directivity of the fiber response with respect of the direction of the particle motion, and the quality of the signal with respect to cable type.

Vertical geophones were deployed every 5 m to provide a comparison along the southeast to northwest side and the west to east side of the triangle. At every 10 m, the array was complemented by two horizontal geophones oriented in the north and east directions. Distances along the fiber-optic cable were mapped to geophone locations (Table 1). Seismic shots were generated using a sledge hammer and steel plate. Three shot sequences were taken along three different directions to assess the response of the system. The first set of shots was every 10 m for 60 m along the first side of the triangular array in the southeast-to-northwest direction. The second set of shots was every 10 m for 30 m along the second side of the triangular array in the west-to-east direction. The third set of shots was every 13 m for 52 m from the southern vertex in the south-to-north direction. At each location, a minimum of three shots were taken. Fourteen separate locations were used with a total of 69 shots from all locations combined. Although many more shots were recorded, we limited our analysis to the first shot at four locations: A, B, C, and D (Fig.2). Locations A is at the northwest vertex and location B is 30 m to the NW of location A. Location C is 13 m north of the south vertex and 39 m farther away in the north direction is location D.

The signals from each shot were recorded by the DAS interrogator over 10-second windows and the geophones over 30-second windows. The interrogator and geophone systems were time synchronized using co-located sensors and first arrivals. The hammer trigger was recorded on the geophone system so zero time for the DAS system was calculated for each shot after time synchronization was performed. DAS data were collected using a 10-kHz sampling rate with the interrogator producing discrete seismic traces every half meter of cable. For our study, a single 30-s record collected at every half meter of the 443-m long cable at 10 kHz sampling rate yields a 266-Megabyte file or about 2 Megabytes per 100 m of cable per second of recording. To help speed up processing and interpretation of the data, the DAS files for each shot were down sampled by a factor of 10 and converted to SEG-Y file format.

Table 1. Cable Mapping of DAS Cable Distance at Co-located Geophones

Location	Channel number	iDAS cable distance for tight-buffered cable (m)	iDAS cable distance for loose tube cable 1st wrap (m)	iDAS cable distance for loose tube cable 2nd wrap (m)	iDAS cable distance for loose tube cable 3rd wrap (m)
0m along S–NW line (South Vertex)	1	24.2	134.55	224.55	314.55
10m along S–NW line	5	34.2	144.55	234.55	324.55
20m along S–NW line	9	44.2	154.55	244.55	334.55
10m along NW–NE line	17	64.2	174.55	264.55	354.55
20m along NW–NE line	21	74.2	184.55	274.55	364.55
Total cable length		111m			334m

An overview of how DAS records data is shown in a 3D plot of amplitude-distance-time of the wave field from the shot 13 m north of the south vertex (Fig. 3). In Fig. 3, the DAS signal was processed with a sample spacing of 0.5 m, so the channel number divided by two represents the distance along the fiber given by the mapping in Table 1. Starting at the south vertex, the arrival time of first arrivals initially decrease as the cable channel number increases to the northwest because the distance from the cable to the source in the middle of the triangle decreases. After passing the midpoint of the line segment between the south vertex and the northwest vertex, travel times increase, according to the geometry of the triangle because P-wave velocity in the ice is fairly uniform. The amplitudes midway between vertices are reduced significantly as the wave propagation direction is perpendicular to the cable. The directional sensitivity of the cable is discussed in a later section of the paper.

Data Conditioning

To ensure high signal-to-noise traces, a check that included an automatic first-arrival picker was used to

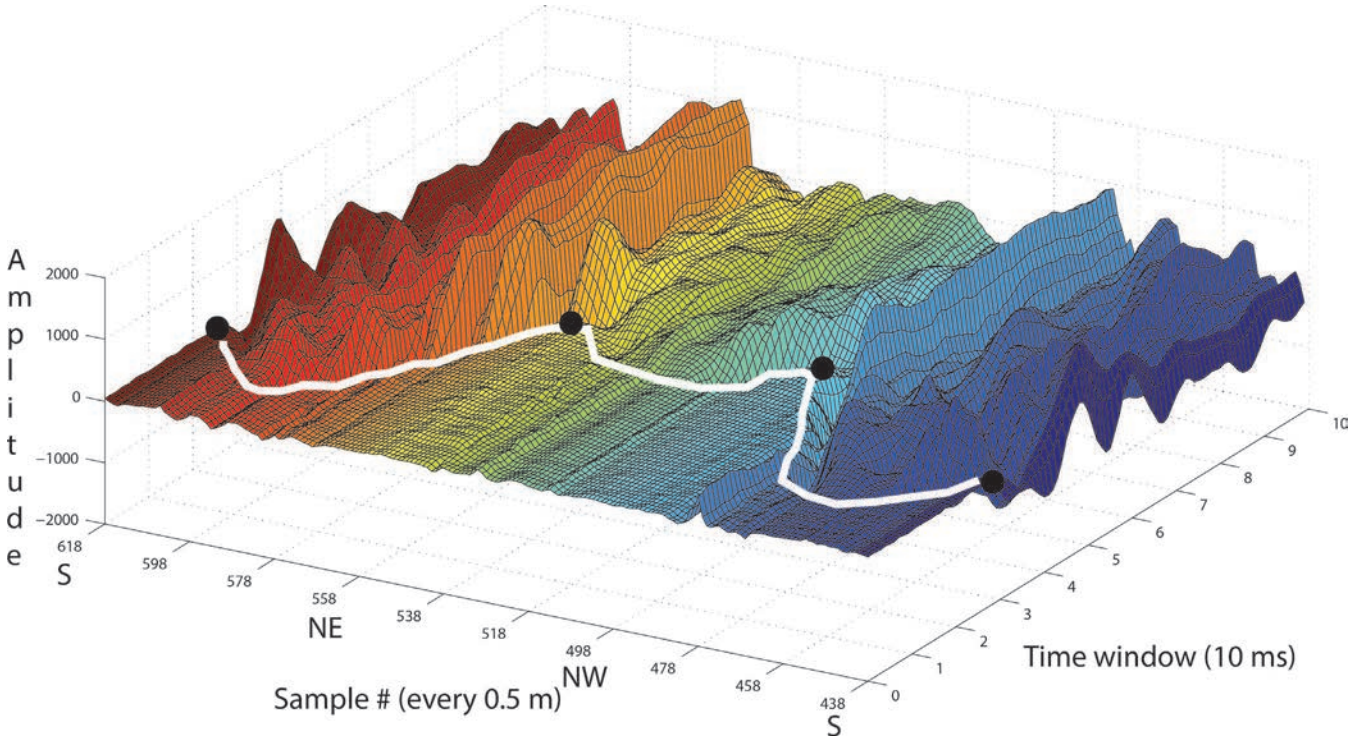

Figure 3. First arrivals from the first wrap of the loose-tube fiber cable from the source location 13 m north of the South vertex of the array (location C in Fig. 2). The trace of the first arrivals is outlined in white. Black dots at South, Northwest, and Northeast show the vertices of the triangular array. The amplitude is in arbitrary units.

Table 2. Statistics of Poor Signal-to-Noise Traces

Source location	Number of tight-buffered fiber cable traces removed and percentage (out of 172)	Number of loose-tube fiber cable traces removed and percentage (out of 601)	Total number of traces removed (out of 773)
A	41 (23.8%)	298 (49.6%)	339
B	54 (31.4%)	318 (52.9%)	372
C	14 (8.1%)	198 (32.9%)	212
D	53 (30.8%)	452 (75.2%)	505

distinguish good traces from bad. First-arrival times were picked using an autoregressive Akaike Information Criterion (AIC) picker. The AIC picker is a type of automatic onset detection algorithm that utilizes a time window around the onset of the signal at the receiver to pick, or identify the determination of the onset time, with high fidelity (Kurz *et al*., 2005). The AIC picker was used to determine the first-arrival times for the geophone data as well as most of the radially-to-obliquely oriented DAS array lines. The picker did encounter problems with the nearly perpendicularly oriented DAS array lines due to the directional sensitivity of the DAS and the low signal-to-noise ratio of these signals. They were identified using a cutoff threshold based on the output from the AIC picker. Then, the DAS dataset was inspected manually to remove remaining bad traces. Good traces ranged from 34.7% to 72.6% of the full data set for the different shots (Table 2). Most of the traces that were removed due to bad picks were from a nearly perpendicularly oriented array line, which is an effect of the directional response of the system. The total recorded cable length of 443 m was relatively short compared to the maximum sensing distance for a single DAS interrogator of 100 km. Therefore, negligible signal-to-noise degradation was expected, and thus observed in the data.

Cable Comparison and Repeatability

DAS can use nearly any single-mode, fiber-optic cable as a distributed array of seismic sensors (Mestayer *et al*., 2011). Recent testing has shown that multi-mode fiber-optic cable can be used as well (Xiao, 2013). Although there are many specialty cables, we focused on investigating the role of coupling between cladding and sheathing on performance by comparing the responses from the two different cable constructions used in our field experiment. Loose-tube construction consists of an optical fiber being placed with a gel inside a hard tube which does not completely transfer external strain to the fiber. Loose-tube is typically used for DTS applications. Tight-buffered construction has an optical fiber being connected, via a plastic buffer, to a hard tube which transfers external strain to the fiber (Iten, 2011). Of the two different constructions, tight-buffered fiber cables are designed to be better suited for elastic wave sensing because they more faithfully transfer the strain on the surface of the cable to the fiber core.

We are comparing in this paper the signal response from the tight-buffered fiber cable to the loose-tube fiber cable. The suitability of loose-tube construction for DAS arrays can be a consideration when an application benefits from combined temperature and acoustic sensing. For the signal comparison, traces from each cable construction at various array locations were examined for similarities. Example comparisons for four different source locations at different cable locations highlight how the tight-buffered cable response was more consistent for the picking of P-wave first arrivals (Fig. 4). Different orientations from source to cable direction are included. For each source-cable location pair, the co-located tight-buffered fiber response and the loose-tube fiber response are plotted together. For all four plots the P-wave first arrival is clear for the tight-buffered fiber and unclear for the loose-tube fiber. At each of these locations the loose-tube response is considered a bad response and was removed from the data. For each source location, a significantly higher percentage of bad traces had to be removed from the loose-tube fiber data than from the tight-buffered fiber data (Table 2). We conclude that the tight-buffered fiber is more consistent at detecting and recording strain changes and is better suited for DAS.

The examination of the repeatability of measurements was done by comparing the first three occurrences of the loose-tube fiber cable co-located close to the northwest vertex of the array for each of the four shot locations presented at a location with good cable-to-ice coupling (Fig. 5). The first arrivals matched very well for each co-located trace. However, some of the rest of the signal response for each co-located trace does not match as well as the nearly identical co-located traces presented

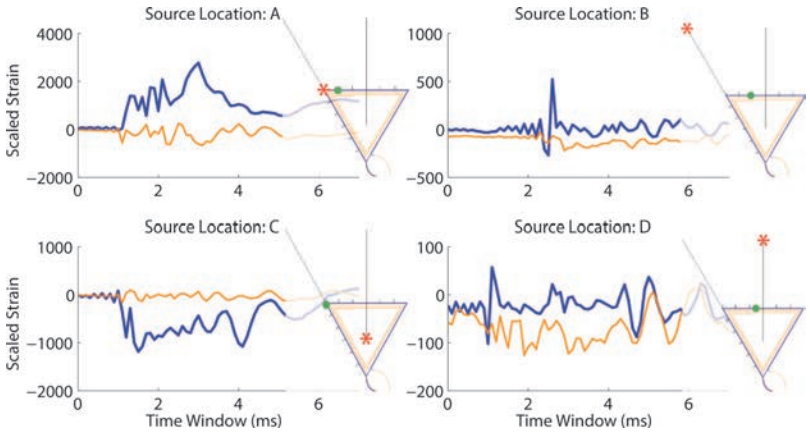

Figure 4. Plots comparing the tight-buffered fiber (thick or blue) and the loose-tube fiber (thin or orange) cables. Traces from each cable are co-located on their first wrap around. Each inset map gives shot location ("*" symbol) and trace location (dot). The y-axis is "Scaled Strain" as they are uncalibrated strain values given in the interrogator. Differences in the "Scaled Strain" values for different shots depend on cable distance and orientation relative to the source.

by Daley *et al*. (2013). A combination of factors associated with cable deployment, lack of data processing, and cable coupling media might explain the differences in the signal response. Most of the DAS array was covered by ice and, in general, had very uniform coupling, although a few locations the coupling was very poor (Fig. 6). The poorly-coupled co-located cable position recorded very different responses and it appears to be responsible for some of the variations in post first-arrival signatures. Sections of melting ice from temperature and sun light variations throughout the day changed the ice conditions that reduced coupling and reduced to quality of some measurements along the array.

Directional Sensitivity

The directional sensitivity of DAS is a feature that is important to consider when designing DAS arrays. If DAS is to be deployed as a large-scale seismic array, the directional sensitivity of the system is essential for the determination of time arrivals of different elastic-wave types. The Lake Mendota array and shot locations were designed to give as many orientations relative to propagation directions as possible to assess the directional sensitivity of DAS. By using the multiple source locations, we observe the DAS amplitude response for P-wave motions in directions that were radial, transverse, and oblique.

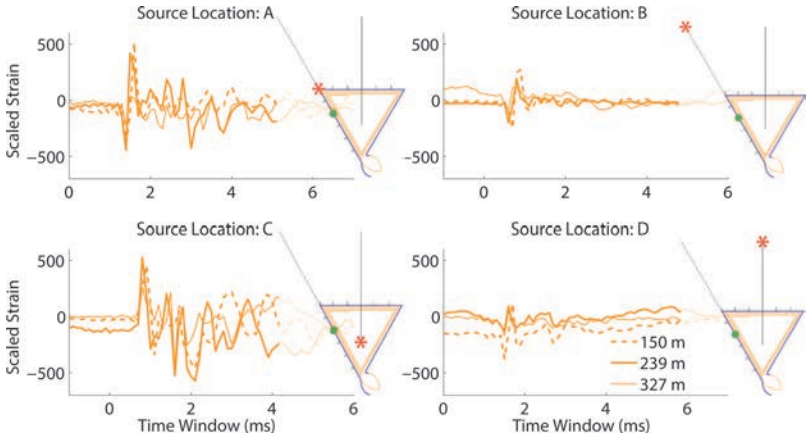

Figure 5. Plots of co-located traces from multiple wraps of the loose-tube fiber cable. Legend numbers in the lower right plot correspond to length of cable from the iDAS interrogator. Traces are co-located from the first three wrap-arounds of the loose-tube fiber cable. Each inset map gives shot location ("*" symbol) and trace location (dot). Differences in the "Scaled Strain" values for different shots depend on cable distance and orientation relative to the source.

Figure 6. Photo of the northwest vertex of the array showing poor cable-to-ice coupling, (*i.e.*, the yellow fiber-optic cable was loose in the air), which will give poor first arrivals.

We first consider a line segment that is oriented in the radial direction of wave propagation. Wiggle traces are shown in Fig. 7 for every channel along the triangle side from the northwest vertex to the south vertex for sources at Locations A and B. The P-wave particle motion is along the cable length, which is the direction in which the fiber-optic cable should be most sensitive. The plots in Fig. 7 contain clear first arrivals with signals above noise level at each location along the cable. Amplitudes of the arrivals for the more distant source B are notably smaller than for the closer source A. The responses are stronger for channels which are closer to the source. The amplitude decays with distance away from the source, which is attributed to geometric spreading and elastic-wave energy loss and not to the light attenuation along the cable. In comparison, Fig. 8 shows wiggle traces along a line segment nearly perpendicular to the source. Wiggle traces are shown along the triangle side from west-to-east between the northwest and northeast vertices for shots C and D. First arrivals are much closer to the noise level for Source C, but are still evident. For Source D, first arrivals are only discernible for channels near the northwest and northeast vertices, whereas first arrivals from locations closer to the center of the line are smaller than the background noise. Amplitudes of P-wave arrivals coming at a nearly perpendicular angle were much closer to the noise level compared with those coming radially (Mateeva *et al.* 2014a). The orientation of the cable line is more important than the distance from the source, which provides useful guidance in designing DAS arrays. Because shots C and D are located along a perpendicular

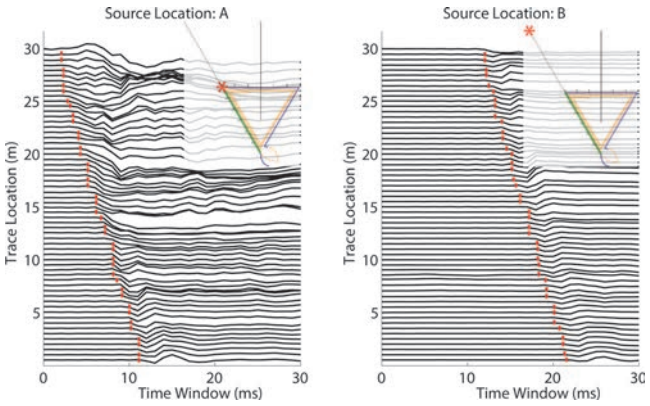

Figure 7. DAS traces along a side of the array aligned with the P-wave ground motion. Plots show each trace along the side between the northwest vertex and the south vertex for source locations A and B. Both array lines are radially oriented relative to propagation direction from each source. First arrivals are picked as vertical lines. The top trace in each plot is closest to each respective source location and the bottom trace is farthest along this array line. Inset map showing the source location ("*" symbol) and northwest vertex to south vertex array line traces is given in the upper right of each plot.

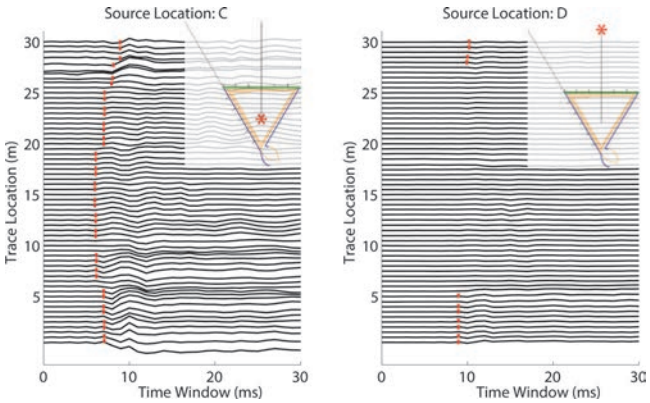

Figure 8. DAS traces along a side of the array aligned obliquely and perpendicularly to the P-wave ground motion. Plots of each trace along the east-west side between the northwest vertex and the northeast vertex for source locations C and D. Both array lines are at a nearly perpendicular orientation relative to propagation direction from each source. First arrivals are picked as vertical lines for each trace from C but are close to the noise level. The visible first arrivals are picked in D showing increasing signal strength moving away from a perpendicular orientation. The center trace in each plot is closest to the respective source location along this array line. Inset map showing the source location ("*" symbol) and northwest vertex to northeast vertex array line is given in the upper right of each plot.

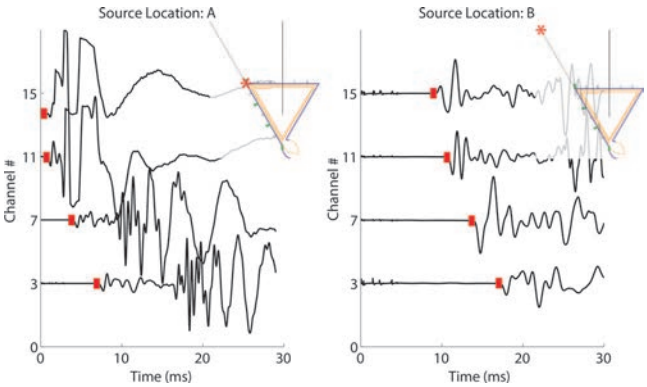

Figure 9. Plots of the horizontal component geophones in line with the respective DAS lines from Fig. 7 for each source location over the first 30 ms of recorded signal. The y-axis gives channel numbers from Fig. 2. Inset map showing the source location ("*" symbol) and component locations (tilted, thicker tick marks) is given in the upper right of each plot. For source locations A and B the horizontal components were rotated to align with the cable direction. Clear P-wave first arrivals, picked (vertical lines), are present for each channel for each source location.

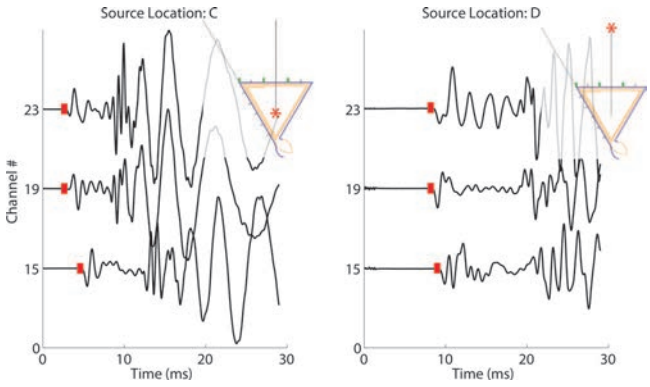

Figure 10. Plots of the horizontal component geophones in line with the respective DAS lines from Fig. 8 for each source location over the first 30 ms of recorded signal. The y-axis gives channel numbers from Fig. 2. Inset map showing the source location ("*" symbol) and component locations (tilted, thicker tick marks) is given in the upper right of each plot. For source locations C and D the East components were used as they were already aligned with the cable. Clear P-wave first arrivals, picked (vertical lines), are present for each channel for each source location.

bisector of the east-west cable segment, the only truly perpendicular cable portion is at the center of this line. As the sensor location moves away from the center, the cable picks up small components of ground motion parallel to its orientation, which is evidenced by the increase in the signal amplitude at the top and bottom of the sequence of traces for both Sources C and D.

In summary, the P-wave response is stronger for a radially-oriented DAS cable than for a perpendicularly-oriented cable. Recording the strongest responses along the radially-oriented sections of cable supports the theory that DAS amplitude is related to the axial strain induced in the fiber core (Parker *et al*., 2014). Thus, DAS sensitivity is highly directional (Parker *et al*., 2014). The directional sensitivity of DAS was further examined using ground motions measured by the reference geophone array. Figures 9 and 10 present traces obtained from the north and east components of the horizontal geophones rotated into the direction of the DAS cable for the same sources shown in Figs. 7 and 8, respectively. Each source location has clear first arrivals above the noise level. Thus, for source locations C and D, the geophone responses in the same direction as the cable are able to pick up the first arrivals where the DAS array was unable to pick first arrivals. This observation provides further support for the interpretation that the weak strength of the first arrival from DAS for perpendicularly-oriented cable is a directional sensitivity effect.

DAS and Geophone Comparison

A preliminary comparison of the DAS data was performed using the reference geophone dataset. For the comparison source location B was used with the rotated horizontal geophone channels 3 and 7 (Fig. 9) along with the corresponding raw DAS traces at the same location (Fig. 11). The two geophone locations are the furthest south three-component geophone locations and are locations well suited for high signal-to-noise DAS responses from source B. Differences in amplitude values and noise characteristics between uncorrelated DAS and geophone datasets are accounted for with plotting the datasets separately. For a full waveform comparison between DAS and geophone data, Daley *et al*. (2015) has shown that stacked and data conditioned DAS data is most appropriate for direct comparison of the complete waveform. For our preliminary comparison between the datasets, first arrival time delay between the two locations was used. Geophone channels 3 and 7 (Fig. 9) and the DAS traces at the same location (Fig. 11) show similar delay times in first arrivals between the two locations with a slightly longer delay time (∼1 ms) on the DAS data. This is due to the distributed nature of

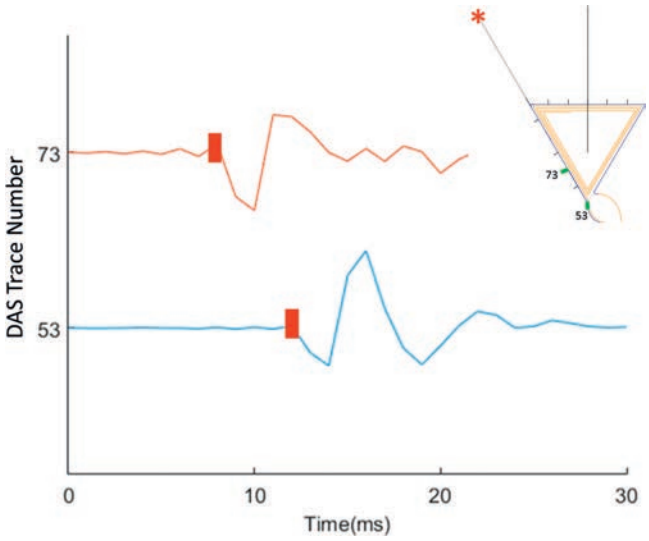

Figure 11. Plots of the DAS traces co-located with rotated horizontal geophone channels 3 and 7 for source location B over a 30 ms window of recorded signal. The y-axis gives the trace number from the DAS system. Inset map showing the source location ("*" symbol) and locations (tilted tick marks) with trace number is given in the upper right. Clear P-wave first arrivals, picked in red tick marks, are present for each channel for each source location.

DAS and that the data is unstacked and thus, not achieving that same geophone spacing even though they are co-located. Daley *et al*. (2015) has performed more robust comparisons between DAS and geophone datasets focusing on signal-to-noise ratios between the two. They have shown that for DAS data, when averaged over a comparable interval to typical geophone spacing, can obtain signal-to-noise ratios of 18 to 24 dB below clamped geophones and is variable due to the noise characteristics not being identical. A spectral response from stacked DAS data would highlight the signal-to-noise ratio differences between the two datasets, but since the DAS data is unstacked it would be unrepresentative of the achievable spectral response. Overall, the raw unstacked DAS data had comparable first arrival time delays with improvement in the DAS data expected if stacking of the data had occurred beforehand.

Summary and Conclusions

Although any type of single-mode, fiber-optic cable can be used for DAS measurements; specialty cables can be more sensitive to variations in strain rates. First arrivals for co-located signals emphasized that cable construction plays a large part in how strain is transferred to the fiber core and subsequently recorded. The first arrivals also showed that any cable type can be used for DAS. The sensitivity of DAS is enhanced when the array is aligned radially with the propagation direction of an elastic wave traveling through the medium. Preliminary comparison of the travel time delay between DAS and the geophone reference survey proved useful in understanding the differences between the nature of the two systems, as well as what steps to take to fully take advantage of the distributed nature of DAS.

DAS technology provides great opportunities to create dense sensor arrays. However, users must properly consider directivity of the sensor, select the right cable type, and establish good medium-to-cable coupling to improve signal responses and improve interpretation of fiber-optic vibration data.

Acknowledgements

The University of Wisconsin-Madison authors would like to thank Joe Greer at Silixa for his contribution in the preparation of this paper. We also thank JoAnn Gage, Chelsea Lancelle, Ashley Meulemans, and Peter Sobol from UW-Madison for their help with the field experiment. This research was supported by the NSF project NSF-CMMI 0900351.

References

Baldwin, J., Fratta, D., Wang, H., Lord, N, Nigbor, R., Chalari, A., Karaulanov, R., Lancelle, C., and Castongia, E., 2014, Using distributed acoustic sensing (DAS) for Multichannel Analysis of Surface Waves (MASW) to evaluate ground stiffness: Abstract NS31C-3938, 2014 Fall Meeting, AGU, San Francisco, Calif., 15–19 Dec.

Daley, T.M., Freifeld, B.M., Ajo-Franklin, J., Dou, S., Pevzner, R., Shulakova, V., Kashikar, S., Miller, D.E., Goetz, J., Henninges, J., and Lueth, S., 2013, Field testing of fiber-optic Distributed Acoustic Sensing (DAS) for subsurface seismic monitoring: The Leading Edge, **32**, 699–706.

Daley, T.M., Miller, D.E., Dodds, K., Cook, P., and Freifeld, B.M, 2015, Field testing of modular borehole monitoring with simultaneous distributed acoustic sensing and geophone vertical seismic profiles at Citronelle, Alabama: Geophysical Prospecting, **64**, 1,318–1,334.

Eisen, O., Hofstede, C., Miller, H., Kristoffersen, Y., Blenkner, R., Lambrecht, A., and Mayer, C., 2010, A new approach for exploring ice sheets and sub-ice geology: Eos, Transactions American Geophysical Union, **91**, 429–430.

Ewing, M., and Crary, A.P., 1934, Propagation of elastic waves in ice. Part II: Journal of Applied Physics, **5**, 181–184.

Iten, M., 2011, Novel applications of distributed fiber-optic sensing in geotechnical engineering: Ph.D. thesis, ETH Zurich, Switzerland.

Johannessen, K., Drakeley, B., and Farhadiroushan, M., 2012, Distributed Acoustic Sensing - a new way of listening to your well/reservoir: SPE Intelligent Energy, 9 p.

Kurz, J.H., Grosse, C.U., and Reinhardt, H., 2005, Strategies for reliable automatic onset time picking of acoustic emissions and of ultrasound signals in concrete: Ultrasonics, **43**, 538–546.

Lancelle, C., Lord, N.E., Wang, H.F., Fratta, D., Nigbor, R.L., Chalari, A., Karaulanov, R., Baldwin, J.A., and Castongia, E., 2014, Directivity and sensitivity of fiber-optic cable measuring ground motion using a Distributed Acoustic Sensing array: Abstract NS31C-3935, 2014 Fall Meeting, AGU, San Francisco, Calif., 15–19 Dec.

Lord, N., Wang, H., and Fratta, D., 2016. A source-synchronous filter for uncorrelated receiver traces from a swept-frequency seismic source: Geophysics, **81**, P47–P55.

Madsen, K. N., Parker, T., and Gaston, G., 2012, A VSP field trial using distributed acoustic sensing in a producing well in the north sea: 74th EAGE Conference & Exhibition incorporating SPE EUROPEC 2012, Copenhagen, Denmark, 4–7 June.

Mateeva, A., Lopez, J., Potters, H., Mestayer, J., Cox, B., Kiyashchenko, D., Wills, P., Grandi, S., Hornman, K., Kuvshinov, B., Berlang, W., Yang Z., and Detomo, R. 2014a. Distributed acoustic sensing for reservoir monitoring with vertical seismic profiling: Geophysical Prospecting, 62, 679–692.

Mateeva, A., Mestayer, J., Yang, Z., Lopez, J., Wills, P., Wu, H., Wong, W., Cox, B., Roy, J., and Bown, T., 2014b, Progress in DAS seismic methods: GeoConvention 2014 Focus.

Mestayer, J., Cox, B., Wills, P., Kiyashchenko, D., Lopez, J., Costello, M., Bourne, S., Ugueto, G., Lupton, R., Solano, G., Hill, D., and Lewis, A., 2011, Field trials of Distributed Acoustic Sensing for geophysical monitoring: SEG San Antonio Annual Meeting, 4,253–4,257.

Mellors, R. J., Pitarka, A., Kuhn, M., Stinson, B., Ford, S. R., Snelson, C., and Drachenberg, D., 2014, Fiber Optic Acoustic Sensing (FOAS) far-field observations of SPE 3: Poster #66, 2014 Annual Meeting, SSA, Anchorage, Alaska, 30 April, Seismological Research Letters, **85**, p. 450.

Miller, D., Parker, T., Kashikar, S., Todorov, M., and Bostick, T., 2012, Vertical Seismic Profiling using a fibre-optic cable as a Distributed Acoustic Sensor: 74th EAGE Conference & Exhibition incorporating SPE EUROPEC, Copenhagen, Denmark.

Molenaar, M.M., Hill, D., Webster, P., Fidan, E. and Birch, B., 2012, First downhole application of distributed acoustic sensing for hydraulic-fracturing monitoring and diagnostics: SPE Drilling & Completion, **27**, 32–38.

Parker, T., Shatalin, S.V., and Farhadiroushan, M., 2014, Distributed Acoustic Sensing – a new tool for seismic applications: First Break, **32**, 61–69.

Parker, T., Shatalin, S.V., Farhadiroushan, M., Kamil, Y.I., Gillies, A., Finfer, D., and Estathopoulos, G., 2012, Distributed Acoustic Sensing - a new tool for seismic applications: 74th EAGE Conference & Exhibition incorporating SPE EUROPEC, Copenhagen, Denmark.

Tronicke, J., Tweeton, D. R., Dietrich, P., and Appel, E., 2001, Improved crosshole radar tomography by using direct and reflected arrival times: Journal of Applied Geophysics, **47**, 97–105.

Wang, H.F., Lord, N.E., Chalari, A., Lancelle, C., Baldwin, J.A., Castongia, E., Fratta, D., Nigbor R.L., and Karaulanov, R., 2014, Field trial of distributed acoustic sensing using active sources at Garner Valley, California: Abstract NS41C-07, 2014 Fall Meeting, AGU, San Francisco, Calif., 15–19 Dec.

Wen, T., Garrison, G.R., Francois, R.E., Stein, R.P., and Felton, W.J., 1991, Sound speed, reflectivity, and absorption measurements in arctic ice in 1988*:* Report Number APL-UW-TR-9005, Washington University, Seattle Applied Physics Lab.

Xiao, J., Farhadiroushan, M., Clarke, A., Khalifa, Q., Mulhem, A., Forero Reyes, H., Parker, T. R., Shawash, J., Milne, H. C., 2013, Inflow monitoring in intelligent wells using Distributed Acoustic Sensor: *In* SPE Middle East Intelligent Energy Conference and Exhibition, 28 Oct.